Microwave transmission in sodium and potassium at 80 GHz in the perpendicular-field geometry

1989 J. Phys.: Condens. Matter 1 875

(http://iopscience.iop.org/0953-8984/1/5/004)

J. Phys.: Condens. Matter 1 (1989) 875–890. Printed in the UK

Microwave transmission in sodium and potassium at 80 GHz in the perpendicular-field geometry

G L Dunifer, J R Sambles† and D A H Mace‡
Department of Physics and Astronomy, Wayne State University, Detroit, MI 48202, USA

Received 25 July 1988

Abstract. We present the results of an experimental investigation of microwave transmission through thin plates of sodium and potassium metal carried out at 80 GHz and 1.3 K in the perpendicular-field geometry. The characteristics of Gantmakher–Kaner oscillations and cyclotron phase resonance are presented. Although the physical causes of these signals are well understood, a number of details do not appear to be adequately described by current theory. We also describe two other classes of signals that are superimposed on the first two, but whose origins are still uncertain.

1. Introduction

This paper is the last in a series of three papers on a detailed study of microwave transmission in thin plates of high-purity sodium and potassium metal. The experimental observations were carried out at cryogenic temperatures at a frequency of 80 GHz on approximately 40 different samples. The samples ranged in thickness from about 15 to 300 μm and were oriented either parallel or perpendicular to a DC magnetic field, whose magnitude could be varied between 0 and 60 kG. The first paper (Mace *et al* 1984) was concerned with the study of spin-wave (SW) modes and the accurate determination of the first three spin-dependent Landau Fermi-liquid parameters B_0, B_1 and B_2. The second paper (Dunifer *et al* 1987) was concerned with the study of cyclotron-wave (CW) modes and the determination of the spin-independent Landau Fermi-liquid parameters A_1, A_2 and A_3. This second class of signal results from the orbital motion of the conduction electrons in the applied magnetic field and is observed in transmission when the field is oriented parallel to the surface of the sample. The purpose of this present paper is to report on the remaining class of transmission signals due to orbital motion which is seen when the field orientation is perpendicular to the sample surface. These signals are in general not as well understood as the SW and CW modes and further theoretical investigation would be useful. Their characteristics, however, are sufficiently well known for us to have used them to calibrate the thicknesses of the samples for the SW analysis in our first paper.

† Present address: Department of Physics, University of Exeter, Exeter EX4 4QL, Devon, UK.
‡ Present address: British Telecom Research Laboratory, Martlesham Heath, Ipswich IP5 7RE, East Anglia, UK.

0953-8984/89/050875 + 16 $02.50

2. Experimental technique

The experimental technique was described in detail in the first two papers. The transmission spectrometer used was described by Dunifer and Pattison (1976). In brief, the experiment was conducted using the microwave transmission technique in which the sample makes up a common wall between two microwave cavities tuned to the same frequency. A DC magnetic field is oriented perpendicular to the plane of the sample. The introduction of microwaves into one of the cavities provides a strong RF electromagnetic field at one of the surfaces of the sample, where conduction electrons passing within a skin depth of that surface are driven by the RF fields present. The other cavity functions as a receiving antenna, collecting any power transported across the sample by the conduction-electron system. This cavity is coupled to a sensitive detector, which is used as a mixer, mixing any transmitted power with a *coherent* microwave reference. The output of this detector, which we call the *signal*, is thus proportional to that component of the transmitted microwave field in phase with the reference. As seen later, it is sometimes useful to spin rapidly the phase of the reference while slowly sweeping the DC magnetic field intensity through any signals present. The envelope of this oscillatory signal is thus proportional to the amplitude of the transmitted microwave field and we call it the *signal modulus*. The microwave cavities used are rectangular cavities excited in the TE_{101} mode. As a consequence the driving fields at the surface of the sample are *linearly* polarised, and the receiving cavity accepts only linearly polarised fields of the same orientation as the driving fields.

The samples were fabricated from high-purity Na and K having bulk residual resistance ratios (RRR) of 5000 to 7000. The temperature could be varied between 1.3 and 40 K; however, most of the data presented here were taken at 1.3 K in order to obtain the largest values of $\omega\tau$, where τ is the average momentum-scattering time. As determined from the SW linewidths (Mace *et al* 1984), the low-temperature value of $\omega\tau$ for a typical K sample was 150 while that for a Na sample was 100. This gives rise to electronic mean free paths, $\lambda = v_F\tau$, of about 210 and 170 μm in K and Na respectively.

The samples were produced in an argon-filled dry box. The alkali metal was first extruded as a thin ribbon, about 10% thicker than that desired for the specimen. The ribbon was then pressed between windows of optically polished, fused quartz reducing the thickness to its final value. For the initial set of samples this was done directly in the argon atmosphere of the dry box. The surfaces of these samples appeared to the eye as brilliant mirrors. However, a microscopic examination of the surface revealed many small bubbles, voids and various defects presumably due to argon gas trapped between the quartz and the alkali metal. The SW spectra of these samples often showed structure resulting from the non-uniform thickness across the sample. In order to improve the surface quality in the final set of samples, the pressing between the quartz windows was done in vacuum. In general this treatment produced a significant reduction in the size of the surface defects and a considerable improvement in the quality of the SW spectra. However, the surfaces remained imperfect and under the microscope even the best samples still displayed some imperfections: a faint milky appearance, numerous small bubbles at the surface (typical diameters of 10–20 μm), and microscopic protrusions due to shallow scratches on the quartz windows.

3. Experimental data and analysis

In table 1 we have listed all of the alkali-metal samples studied in the perpendicular-field geometry. The sample numbers are the same as those used in Mace *et al* (1984). Listed

Table 1. A summary of samples used in this study.

Material	Sample	Frequency (GHz)	L_{direct} (μm)	Low-field L_{GKO} (μm)	High-field L_{GKO} (μm)	CPR $m\dagger/m_0$	ΔH_{HFO} (G)	Number of CPR subharmonics
Potassium	K-1†	78.85	140 ± 5	138 ± 3	—	—	945 ± 8	2
	K-2	78.78	104 ± 2	107 ± 2	111 ± 3	—	857 ± 11	2
	K-3†	79.28	85 ± 5	85 ± 4	101 ± 4	1.233 ± 0.003	795 ± 14	2
	K-4	79.18	85 ± 5	86 ± 2	93 ± 3	1.233 ± 0.004	639 ± 5	3
	K-5†	79.18	85 ± 3	73 ± 3	79.3 ± 1	1.217 ± 0.002	828 ± 18	1
	K-7†	79.37	56 ± 2	52 ± 4	64 ± 4	1.219 ± 0.002	806 ± 6	3
	K-8	78.89	168 ± 2	168.3 ± 0.6	168.5 ± 0.8	1.218 ± 0.003	627 ± 6	2
	K-10	79.41	23 ± 2	—	—	1.221 ± 0.001	—	—
	K-12	79.80	41 ± 3	29.0 ± 1.5	—	1.221 ± 0.002	—	4
	K-16‡	79.43	168 ± 2	169.7 ± 0.8	170.1 ± 0.5	1.242 ± 0.01	—	2
	K-19‡	79.38	272 ± 2	272.7 ± 1	272.6 ± 1.2	1.249 ± 0.01	495 ± 15	2
	K-20‡	79.20	271 ± 2	273 ± 2	286.8 ± 1	1.217 ± 0.004, 1.255 ± 0.003		1
	K-24‡	80.06	131 ± 2	130.1 ± 0.5	134.4 ± 0.5	1.228 ± 0.003	603 ± 15	2
	K-25‡	79.86	94 ± 2	95.8 ± 1.5	101.5 ± 1	1.2202 ± 0.0005, 1.231 ± 0.001	—	1
	K-26‡	80.03	28 ± 3	24.3 ± 0.5	—	1.2194 ± 0.0008	—	3
Sodium	Na-1	79.05	172 ± 2	—	—	1.303 ± 0.005	730 ± 20	0
	Na-5‡	80.02	133 ± 2	132.2 ± 0.9	131 ± 2	1.244 ± 0.005, 1.286 ± 0.005	—	1
	Na-6‡	80.05	84 ± 2	84.6 ± 0.3	84.4 ± 3	1.247 ± 0.003, 1.284 ± 0.01	—	1
	Na-7‡	80.12	110 ± 2	109.4 ± 0.7	111.0 ± 1.5	1.252 ± 0.005	—	0
	Na-8‡	80.04	101 ± 2	101.9 ± 0.5	101.5 ± 1	1.247 ± 0.003, 1.294 ± 0.01	—	1
	Na-11‡	80.08	18 ± 3	14.0 ± 0.3	—	1.255 ± 0.002	—	1

† Considerable distortion of sw spectra.
‡ Sample fabricated in vacuum.

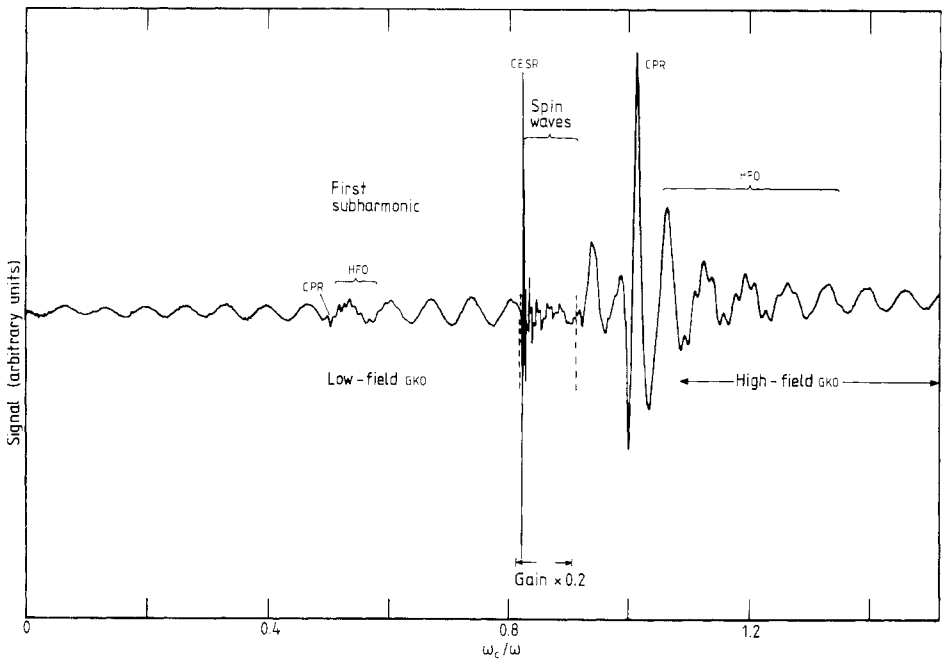

Figure 1. The transmission signal in sample K-24 at 1.3 K as a function of ω_c/ω. An arbitrary choice of the microwave reference phase has been used. Note the decrease of gain in the vicinity of the spin signals.

for each sample are the observation frequency, the sample thickness as measured directly by the micrometer and a series of other quantities as determined from the data and discussed individually in the following subsections. The micrometer measurement was made at room temperature (295 K) and corrected for thermal contraction to 1.3 K (4.15% for K and 3.60% for Na; see Dunifer *et al* 1974). The samples marked with a single dagger (†) are those whose SW spectra showed considerable distortion, such as a splitting into two or more components, which we have interpreted as a non-uniformity of the thickness. The samples marked with a double dagger (‡) are those that were fabricated in vacuum and have the higher-quality surfaces.

In figure 1 we illustrate the different types of signal observed in this geometry. The figure shows the transmission signal in sample K-24 as the magnetic field is swept from 0 to 52.6 kG. The field is expressed in terms of the dimensionless quantity ω_c/ω where $\omega_c = eH/m^*c$ is the cyclotron frequency of the conduction electrons as determined by their effective mass m^*. For the effective mass we have used the most precise values available, which are obtained from the de Haas–van Alphen (DHVA) effect: $m^*/m_0 = 1.211 \pm 0.005$ for K (Abd El-Rahman *et al* 1985) and $m^*/m_0 = 1.256 \pm 0.003$ for Na (Elliott and Datars 1982).

The conduction-electron spin resonance (CESR) and associated SW modes lie in the region $0.8 \leqslant \omega_c/\omega \leqslant 0.9$. For display purposes, the gain in this region has been reduced by a factor of five due to the strength of the spin signals. Close to $\omega_c/\omega = 1$ is a rather strong transmission signal known as the cyclotron phase resonance (CPR). The general oscillatory signal seen over most of the field sweep are the Gantmakher–Kaner oscil-

lations (GKO). The GKO, in fact, extend over the entire field range but are most clearly seen for fields below the CESR (where we will refer to them as the low-field GKO) and for fields that lie above the CPR (where we will refer to them as the high-field GKO). Superimposed on the high-field GKO immediately above the CPR is a higher-frequency oscillation (HFO), which is not present in all samples. And finally, superimposed on the low-field GKO can be seen in general one or more subharmonics of the CPR and HFO. Each of these signals, except for the spin signals, will now be discussed individually.

3.1. Gantmakher–Kaner oscillations

GKO, which were first observed and explained by Gantmakher and Kaner (1965), have been studied previously in the alkali metals at microwave frequencies of 9 GHz (Pinkel *et al* 1978) and 116 GHz (Phillips *et al* 1972a). They are sinusoidal oscillations in the transmission signal as a function of the applied magnetic field due to the changing characteristics of the RF current flowing on the emergent face of the sample as the field intensity is swept. An *approximate* view of the physical process is given by considering those electrons on the spherical Fermi surface whose velocity directed along the field is v_H. The electrons are driven at the incident surface of the sample by the linearly polarised RF electric field present. The helical trajectory of the electrons in crossing a sample of thickness L will cause the plane of polarisation of the induced current to rotate through an angle $\theta = \omega_c L/v_H$ as it traverses the sample. As a consequence, the transmission signal produced by this group of electrons will be given by:

$$dS = C\,dJ(v_H)\cos\left(\frac{\omega_c L}{v_H}\right)\cos\left(\frac{\omega L}{v_H} - \varphi_{ref}\right) \tag{3.1}$$

where C is a constant of proportionality and $dJ(v_H)$ is the current flowing on the emergent face due to these electrons. The first cosine factor gives that component of the radiated field accepted by the receiving cavity, while the second takes into account the phase difference which develops between that of the radiated field and that of the microwave reference φ_{ref} while the electrons are traversing the sample. Equation (3.1) can also be written as

$$dS = \frac{C\,dJ(v_H)}{2}\left[\cos\left(\frac{(\omega+\omega_c)L}{v_H} - \varphi_{ref}\right) + \cos\left(\frac{(\omega-\omega_c)L}{v_H} - \varphi_{ref}\right)\right]. \tag{3.2}$$

In this form the two terms represent the response of the electrons to the two circular components of the linearly polarised driving field. The net signal is found by integrating the effect over the Fermi surface; i.e. letting v_H vary from zero to v_F. Unless one is near cyclotron resonance ($\omega = \omega_c$), the contributions from the various groups of electrons tend to cancel out because of the various phases resulting from the different values of v_H. This leaves a weak signal coming from the extremal electrons at the tip of the Fermi surface:

$$S = C\cos\left(\frac{\omega_c L}{v_F}\right)\cos\left(\frac{\omega L}{v_H} - \varphi_{ref}\right). \tag{3.3}$$

This is the GKO signal which oscillates linearly with the magnetic field strength. On the other hand, at cyclotron resonance the second term in (3.2) becomes independent of v_H.

Thus all groups of electrons on the Fermi surface can contribute in phase with each other and a strong transmission signal results. This is the CPR and represents a resonance of one of the circular components of the GKO which takes place when $\omega = \omega_c$. The predictions of this simple model then are:

(i) in the vicinity of cyclotron resonance—a strong transmission signal due to a radiated field that is circularly polarised;

(ii) away from cyclotron resonance—a weak oscillatory signal due to a radiated field that is linearly polarised.

The polarisation characteristics of the transmission signal are easily determined by varying φ_{ref}. For linear polarisation, as described by (3.3), there will be a particular phase of the reference for which the signal is zero at all fields. A rotation of φ_{ref} by 90° will then produce a simple cosine oscillation with field having a maximum amplitude. If φ_{ref} is rotated continuously to produce the signal modulus, a standing wave pattern is produced with 'nodes' equally spaced in the field. Equation (3.3) is replaced by

$$S = C\cos\left(\frac{(\omega \pm \omega_c)L}{v_F} - \varphi_{ref}\right) \tag{3.4}$$

for a circularly polarised signal away from the CPR. In this case a rotation of φ_{ref} produces only a phase shift in the oscillation pattern, but its amplitude remains constant. The signal modulus, likewise, will have a constant amplitude in all fields.

It should be mentioned that the simple picture that gives rise to (3.3) and (3.4) is a gross simplification of the actual situation. Much more detailed calculations (see, for example, Baraff (1974) and references therein) show that in order to obtain the actual lineshape of the signal, particularly in the region of the CPR, it appears necessary to perform a self-consistent calculation taking into account both the nature of electron scattering at the surfaces and electron–electron interactions. Nevertheless, far from the CPR the simple description given above appears adequate to give the correct period of the oscillation and the expected polarisation of the signal. From (3.3) or (3.4) the spacing in field between adjacent maxima of the GKO pattern is:

$$\Delta H = 2\pi cm^* v_F/eL = (hc/e)k_F/L \tag{3.5}$$

which depends only on the Fermi wavevector and the sample thickness. For a known thickness L, the period may be used to calculate k_F, or alternatively, as we have done, the previously determined value of k_F may be used to calculate the sample thickness itself.

For the arbitrary value of φ_{ref} chosen in figure 1, the GKO spectrum is quite typical of that seen in other Na and K samples: a low-field GKO whose amplitude is roughly constant or slowly growing with increasing field, and a high-field GKO whose initial amplitude near the CPR is considerably stronger than that at low fields but which decreases back towards the low-field values at our highest fields. In figure 2 we show a more detailed version of the low-field GKO in this sample taken in three different ways. In trace A φ_{ref} is chosen to maximise the signal near zero field; in trace B φ_{ref} is rotated 90° relative to A to minimise the signal near zero field; and in trace C φ_{ref} is rotated continuously to produce the signal modulus. In A the GKO amplitude remains approximately constant over the range $\omega_c/\omega = 0 \rightarrow 0.8$, as expected for linear polarisation. However, in B the signal does not remain zero at all fields but increases with field, beginning at $\omega_c/\omega \simeq 0.15$ and reaching a value near that of A by the end of the sweep. Likewise, the signal

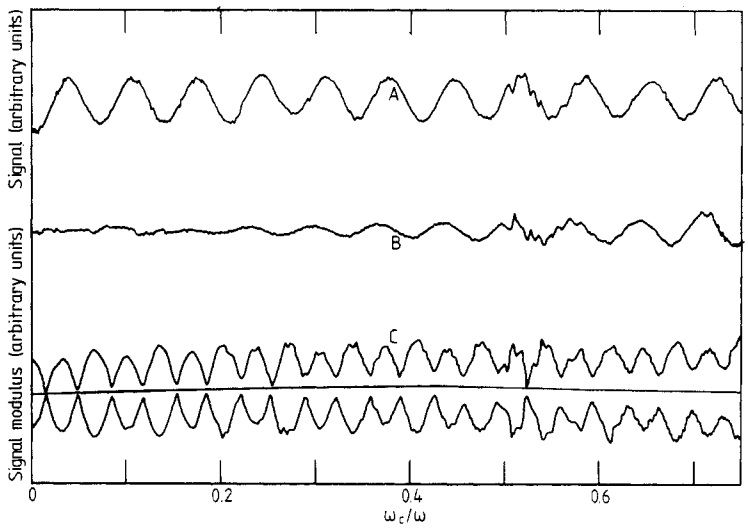

Figure 2. The low-field GKO spectra obtained from sample K-24 at 1.3 K. Trace A, φ_{ref} chosen to maximise the signal near zero field; trace B, φ_{ref} chosen to minimise the signal near zero field; trace C, the signal modulus. (A small distortion is present here due to the accidental leakage of microwaves around the sample. This manifests itself in the alternation of the amplitude between successive 'anti-nodes'.)

modulus in C progresses from the characteristics of linear polarisation at zero field towards those of circular polarisation as the field is increased. This is the situation in both Na and K samples; generally between $\omega_c/\omega = 0.5$ and 0.8 the GKO take on the characteristics of primarily circularly polarised waves. The high-field GKO appear nearly 100% circularly polarised for all fields in the range $\omega_c/\omega = 1.2$–1.7. The reason for this conversion of linear input to circular output at higher fields is not understood.

One possible explanation is that this might be only an artefact due to a non-uniform thickness L. With a range of different thicknesses in a sample, the first cosine factor in (3.3) would give rise to a gradual washing-out of the oscillation in the signal modulus with increasing field. This explanation seems very unlikely since such a variation in L would also cause the overall amplitude of the GKO to diminish with increasing field. We have, however, observed several samples in which the GKO amplitude, with φ_{ref} chosen as in figure 2(*a*), remains nearly constant over the whole range $\omega_c/\omega = 0$–1.7, except, of course, in the region of the CPR. Furthermore, the presence in many samples of very sharp SW structure that can be fitted exactly to theoretical lineshape computations (out to wavevectors in excess of 10^4 cm^{-1}) also indicates a very high degree of uniformity in L.

Another possibility is that the circular polarisation observed is simply the wings of the CPR. This also seems quite unlikely. If the CPR is described approximately by a Lorentzian, then its half-width

$$\Delta(\omega_c/\omega) \simeq 2/\omega\tau \simeq 10^{-2}$$

at our frequency and it is a very localised feature. Even in the 9 GHz observations the linear polarisation had clearly returned within ±2 kG of the CPR (see figure 21 of Pinkel *et al* 1978). Also, a semi-empirical formula suggested by A R Wilson (see equation (3) of Pinkel *et al* 1978), which fits the data well at 9 GHz, predicts no significant circular

polarisation for

$$|\omega_c/\omega - 1| \geq 0.2.$$

This extensive presence of circular polarisation in the radiated field thus appears real and is very different from what was observed at 9 GHz. The signal modulus displayed in figure 22 of Pinkel *et al* (1978) clearly shows the polarisation at the lower frequency to be almost entirely linear over the range $\omega_c/\omega = 2$–5. At their highest field of 20 kG, which corresponds to $\omega_c/\omega \simeq 0.6$ at our frequency, we always detect significant circular polarisation. This suggests that the effect is not associated with the strength of the magnetic field itself, but perhaps with the very large values of $\omega\tau$ achieved in our experiments: $\omega\tau = 100$–150 versus 10–15 at 9 GHz. Further evidence that this may be the case comes from an observation of GKO in copper at 35 GHz for single crystals having RRR $\simeq 20000$ (Phillips *et al* 1972b). For this experiment, $\omega\tau$ was also about 150 and the GKO showed this same feature of evolving from linear to circular polarisation as the field was increased.

Although the polarisation characteristics of the GKO remain unexplained, it was possible to use the period of the oscillations in field to calculate the sample thickness via (3.5). The values of k_F used in the equation were $(0.7446 \pm 0.001) \times 10^8\ \text{cm}^{-1}$ and $(0.9226 \pm 0.0002) \times 10^8\ \text{cm}^{-1}$ for K and Na, respectively, as determined from the low-temperature lattice constant and assuming one conduction electron per atom (see table 1 in Mace *et al* 1984). When possible, the GKO spectra were recorded in the three ways illustrated in figure 2, although sometimes excessive microwave leakage prevented the signal modulus from being obtained. The best estimate of the sample thickness was then obtained by averaging the results of the different methods. This average was generally in agreement with the individual determinations to within $\pm 0.5\%$. In this manner, the thickness L was determined from both the low-field and the high-field GKO individually. The results are listed in table 1 where they are compared with L as measured directly with the micrometer. In some of the thinnest samples it was not possible to make accurate determinations of L from the high-field GKO due to the small number of oscillations available. Also, no determination could be made for sample Na-1, whose thickness was too large for the appearance of GKO.

With the exception of two cases (samples K-5 and K-12), L determined from the low-field GKO is in basic agreement with the direct measurement. The two exceptions almost certainly represent situations in which an error was made in the direct measurement. Sample K-5, for example, presented difficulties because of excess vacuum grease in one of the microwave cavities. The high-field and low-field GKO are in good agreement with each other for all the Na samples. The high-field GKO for K, however, are rather puzzling. For three samples (samples K-8, K-16 and K-19), the high-field and low-field GKO are in excellent agreement. However, for all the other samples, the L-determinations from the high-field GKO are several per cent greater than those from the low-field data, often by considerably more than would be allowed for by the uncertainties in the measurement. Furthermore, there seems to be no correlation between the agreement or disagreement of the low-field and high-field GKO and any other characteristic of the sample, such as the quality of SW spectra, presence or absence of HFO, thickness, method of sample fabrication etc. The only obvious difference between the two classes of GKO signals is that the low-field ones are fairly constant in amplitude, whereas the high-field ones start off quite strong after the CPR and diminish in amplitude rather quickly at first. Nevertheless, they are still linearly spaced in field and in several cases (considering both

Na and K) do give the correct L! Although we have no explanation for this at the moment, it appears that the low-field GKO can be used reliably to determine sample thickness; the high-field ones cannot, at least not in K. As a consequence we have used only the low-field GKO in making our best determination of L for the SW analysis in the perpendicular-field geometry (Mace *et al* 1984). In general the quality of the GKO data allowed this to be done to a precision of $\pm 0.5\%$ or better. Furthermore, this process produced sets of experimental SW disperison relations, the self-consistency of which required an overall accuracy of the same $\pm 0.5\%$ in the L-determinations.

3.2. Cyclotron phase resonance

The CPR is a signal that shows considerable variation from sample to sample. Some of the apparent variation undoubtedly results from the overlap of the CPR with the higher-wavevector SW spectra and the HFO when present. Nevertheless, even samples of comparable thickness, whose other spectra are quite similar, may have quite differently appearing CPR signals. The CPR signal modulus may appear as a single peak that is symmetric, a single peak that is asymmetric with a low-field tail, or a single peak that is asymmetric with a high-field tail. It may also appear as a double peak. In order to be more quantitative, we have defined a CPR mass $m^\dagger$ from the magnetic field H_{CPR} corresponding to the maximum signal modulus:

$$m^\dagger/m_0 = H_{CPR}/H_0 \tag{3.6}$$

where m_0 is the free-electron mass and H_0 is the magnetic field at which cyclotron resonance would take place for free electrons driven at the same microwave frequency. The CPR mass ratio $m^\dagger/m_0$ is listed for each sample in table 1, with two entries being given when there is a well defined double peak.

Although there are several exceptions, the general behaviour is as illustrated in figure 3:

(i) In the thinner samples there tends to be a single, strong, narrow peak, usually quite symmetrical, which has the smallest mass ratio observed: $m^\dagger/m_0 = 1.219 \pm 0.002$ for K, and $m^\dagger/m_0 = 1.248 \pm 0.003$ for Na.

(ii) In the thicker samples there tends to be a single, relatively weak and broad peak, which is asymmetric and has a high-field tail. These have the largest mass ratios observed: $m^\dagger/m_0 \simeq 1.25$ for K and $m^\dagger/m_0 \simeq 1.30$ for Na.

(iii) In samples of intermediate thickness, there tends to be a CPR with a double peak corresponding to mass ratios lying between those of the previous two cases. The most straightforward interpretation of these characteristics is that there are two peaks: a narrower, but more rapidly attenuated peak, associated with the smaller mass ratio, which dominates in the thinnest samples; and a broader, less strongly attenuated peak, associated with the larger mass ratio, which dominates in the thickest samples. For some intermediate thicknesses the two peaks would superimpose with comparable amplitudes, but might still be resolved individually. In this case the apparent mass ratios would move towards each other due to the interference of each peak on the other. If the two peaks could not be resolved individually, then their superposition should produce a single peak corresponding to some intermediate mass ratio. All of this is consistent with the general trends of our observations. It is also observed that as the temperature is raised, the CPR mass ratio tends to increase, again suggesting

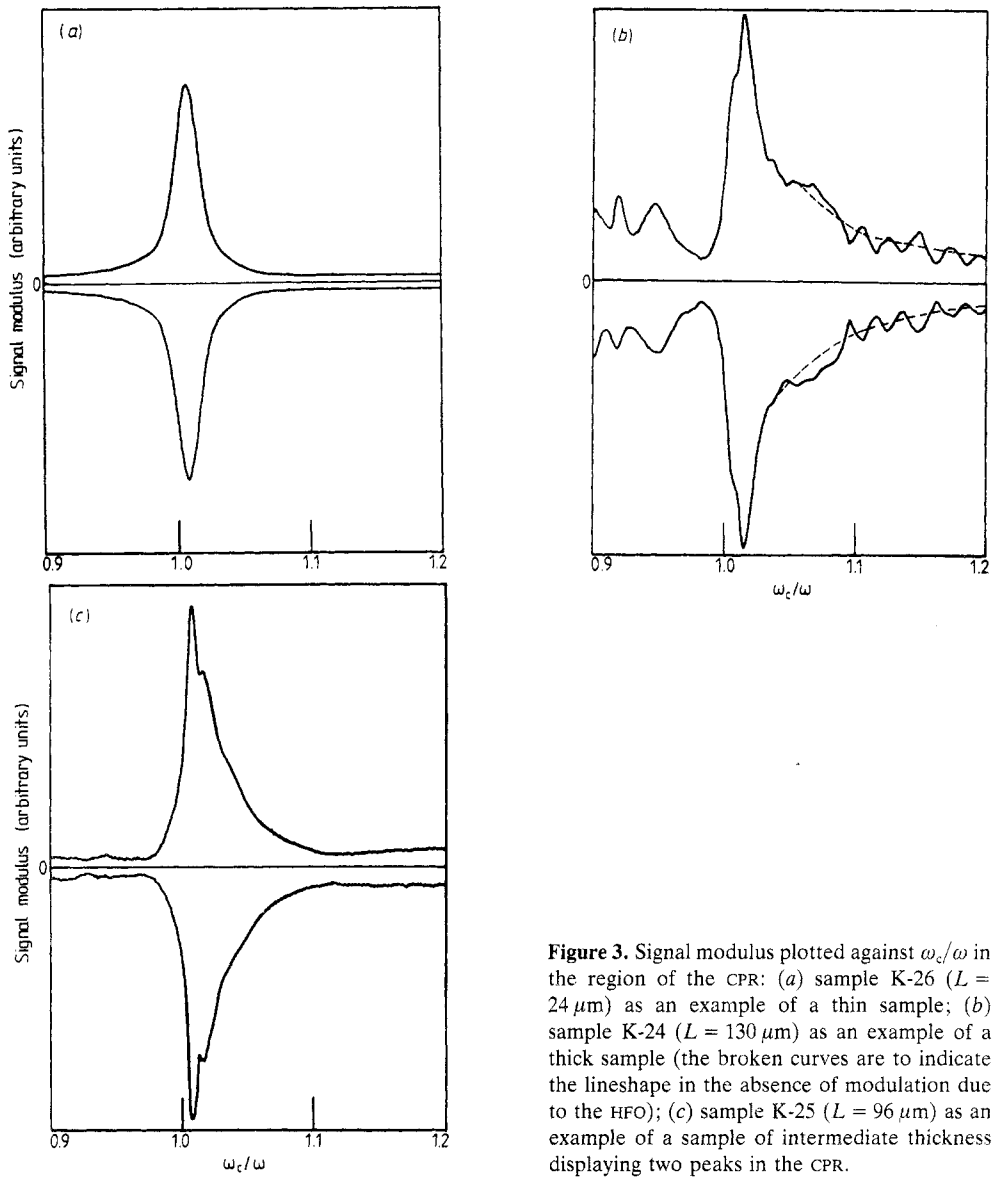

Figure 3. Signal modulus plotted against ω_c/ω in the region of the CPR: (*a*) sample K-26 ($L = 24\,\mu$m) as an example of a thin sample; (*b*) sample K-24 ($L = 130\,\mu$m) as an example of a thick sample (the broken curves are to indicate the lineshape in the absence of modulation due to the HFO); (*c*) sample K-25 ($L = 96\,\mu$m) as an example of a sample of intermediate thickness displaying two peaks in the CPR.

that the contribution of the low-field peak is attenuated more rapidly than that of the high-field one.

In comparing our data with those obtained at 9 GHz (Pinkel *et al* 1978), we find some similarities, but a number of differences as well. At the lower frequency, the CPR is always a single peak with a rather high degree of symmetry. This corresponds most closely with the features seen in our thinnest samples. In fact, the values of $m^{\dagger}/m$ determined at 9 GHz (1.22–1.23 for K and 1.25–1.26 for Na) are in basic agreement with those obtained in our thinnest samples. Furthermore, in these samples it is noted that the choice of φ_{ref}, which produces a symmetric CESR signal, gives rise to an antisymmetric CPR, and vice versa, the same as is observed at the lower frequency.

The major differences develop of course with our thicker samples and the appearance of double peaks or asymmetric peaks with extended high-field tails.

As mentioned earlier, the low-frequency data were compared with a semi-empirical formula suggested by A R Wilson. The formula made use of two different momentum-scattering times—one valid for the bulk of the material and the other, a shorter time, characteristic of a thin layer at each surface. By suitably adjusting the two collision times, it was possible to get quite a good fit to the low-frequency data over the entire range $\omega_c/\omega = 0$–5, thus covering both the GKO and the CPR spectra. Because the Wilson formula produces a CPR with a high degree of symmetry in the signal modulus, it can describe at most only our observations in the thinnest samples. Even for these samples it must fail as the CPR merges into the normal GKO, since it will not predict correctly the circular polarisation that we observe. Thus overall the Wilson formula appears to be of somewhat limited value at our frequency.

Our present data correspond more closely to those obtained in Na and K at 116 GHz (Phillips *et al* 1972a). The RRR of the K in that measurement was somewhat larger than that for our material leading to values of $\omega\tau$ as large as 300. Only a small number of samples were studied, however, and they were all relatively thin ($L \simeq 30$–$70\ \mu$m). These higher-frequency experiments also produced a sharp CPR and an asymmetrical enhancement of the GKO amplitude on the high-field side of the CPR. Also, somewhat more structure was seen in the vicinity of the CPR, which was interpreted as notches in the transmission amplitude. The values of $m^\dagger/m_0$ determined from the CPR peak were 1.228 ± 0.002 for K and 1.25 (no uncertainties listed) for Na. These numbers are again in close agreement with those obtained at the other two frequencies, although the K value is somewhat larger than that calculated in our thinnest samples. We do not detect in our data any consistent features that can be described as notches occurring at fixed values of ω_c/ω.

There are a number of questions that arise concerning the characteristics of the CPR: why is the value of $m^\dagger$ different from that of m^* determined from Azbel–Kaner cyclotron resonance or the dHvA effect (the latter two being in agreement with each other)? What causes the asymmetry of the GKO amplitude on opposite sides of the CPR at high frequency? Are there actually two peaks at high frequency and, if so, what causes them? What was the source of the notches in the transmission amplitude at 116 GHz? And so on. In an attempt to obtain a better understanding of the CPR, Baraff has undertaken an extensive theoretical investigation of microwave transmission in the perpendicular-field geometry (see Baraff (1974) and references therein). He has studied both free-electron and interacting-electron models and the effects of different types of boundary conditions such as specular scattering of the electrons at the surface, diffuse scattering and the influence of rough surfaces. The calculations in closest agreement with the data are those performed for an interacting-electron system as described by the Landau Fermi-liquid theory (Pines and Nozieres 1966). Two different approaches were tried, both of which included the effects of the spin-independent Landau Fermi-liquid parameters A_1 and A_2. By including finite values for A_2 in the calculation, one allows for the propagation of the correlation-produced magnetoplasma mode (CMM mode) first predicted by Cheng *et al* (1968). The CMM mode, in the limit of infinite $\omega\tau$, propagates only over a narrow range of field given by

$$1 - A_2/(1 + A_2) \leqslant \omega_c/\omega \leqslant 1 - 5A_2/3(1 + A_2)$$

which becomes $1.03 \leqslant \omega_c/\omega \leqslant 1.05$ for $A_2 = -0.03$, its approximate value in Na and K (Dunifer *et al* 1987). Baraff *et al* (1969) report experimental evidence of this mode seen in reflection studies of the surface impedance of K at 24 GHz, although Lacueva and Overhauser (1986) have also interpreted the data using a charge-density wave (CDW) model.

The first theoretical approach of Baraff, which he calls his heuristic treatment, was used to interpret the original observations at 116 GHz. According to this approach, the transmission signal is proportional to $\sigma_\infty(L)$ where $\sigma_\infty(z - z')$ is the translationally invariant infinite-medium non-local conductivity. This formulation was unable to account for a number of features in the data, but its derivation contained several physical assumptions that could not be rigorously justified. According to the calculation, the CPR should occur at $\omega_c/\omega = (1 + A_1)^{-1}$. If correct, this would explain the reason for the difference between $m^\dagger$ and m^*, and also allow one to determine the value of A_1 in the alkali metals for the first time. However, the values deduced for A_1 ($|A_1| \simeq 0.01$) were considerably lower in magnitude than their theoretical estimates in these metals ($A_1 \simeq 0.04$–0.10) (Rice 1968). The theory was able to account for the enhanced high-field GKO amplitude as a many-body effect resulting from the negative value of A_2. Finally, the theory was also able to account for the dominant notch in the transmission amplitude as an effect due to the CMM mode. Surprisingly, the theory predicted a reduction rather than an enhancement of the transmission under the conditions necessary for the propagation of this mode.

The second theoretical approach (Baraff 1974) was a numerical self-consistent variational calculation for an interacting-electron system in which the quasi-particles undergo diffuse scattering at both boundaries of the specimen. This calculation, which was performed in an attempt to justify the conclusions of the heuristic treatment, made far fewer assumptions, was much more rigorous overall and presumably should have been a better description of the physical measurement. The results were rather different, however, with the only major feature in common with the first calculation being the enhancement of the high-field GKO relative to the low-field GKO. This again was due to the parameter A_2 and its negative sign. The second method predicted CPR at $\omega_c/\omega = 1.0$, with no shifts due to A_1. Furthermore, it predicted that the effects of the CMM mode should give rise to an enhancement in the microwave transmission, with the maximum enhancement occurring at the high-field cut-off of the mode, $\omega_c/\omega \simeq 1 - \frac{5}{3}A_2 \simeq 1.05$. The theory thus predicts the possibility of two peaks—one associated with the CPR and the other associated with the CMM mode. According to the calculation, the attenuation length for the CMM mode is always less than the electronic mean free path λ, which determines the attenuation length for the CPR and GKO. Consequently, the effects of this collective mode should be strongest in the thinnest sample. In figure 3 of Baraff (1974) the signal modulus is plotted against ω_c/ω for L/λ ranging from 2.0 to 0.1. For $L/\lambda = 2.0$ and 1.0, two distinct peaks are seen in the modulus, with the CPR at $\omega_c/\omega = 1.0$ being the stronger in the thicker sample, but with the CMM mode at $\omega_c/\omega = 1.05$ being stronger in the thinner one. For the thinnest sample, $L/\lambda = 0.1$, the CMM mode completely dominates and only a single peak is seen at $\omega_c/\omega = 1.05$. Finally, this calculation shows that overall the effects of A_1 are rather minor, producing only small lineshape distortions rather than a shifting of any features in the transmission spectrum, which could be used to identify its value.

In comparing our data with Baraff's variational calculation, it might initially appear that there is a correlation between the two peaks that we appear to see and the two peaks predicted by theory. However, there is a serious problem with the thickness

dependence. In our observations it is the low-field peak ($m^{\dagger}/m_0 \simeq 1.22$ or $\omega_c/\omega \simeq 1.01$ in K) that dominates in thin samples, and the high-field peak ($m^{\dagger}/m_0 \simeq 1.25$ or $\omega_c/\omega \simeq 1.03$ in K) that dominates in thick samples. On the other hand, in the theoretical computation, it is the CMM mode ($\omega_c/\omega \simeq 1.05$) that dominates in thin samples and the CPR ($\omega_c/\omega = 1.0$) that dominates in thick samples. Hence it is rather difficult to ascribe one of our peaks to the CPR and the other to the CMM mode. Another difficulty is that the enhancement of the high-field GKO amplitude is greatest in thin samples according to theory, whereas in our data we tend to see this in the thicker samples. It appears that the thickness dependence measured experimentally is the inverse of that predicted theoretically! Qualitatively at least the signals plotted in figures 4, 5, 6 and 8 of Baraff (1974) for a thin sample and a fixed value of φ_{ref} look quite similar to our observations in several of the thicker samples. Baraff's computation was done assuming circular polarisation of the driving field. It would be interesting to superimpose on his present calculation a similar plot for negative ω_c/ω and thus obtain the response to a linear driving field. In particular it would be interesting to see if the enhancement effect of A_2 might account for the polarisation characteristics of our data and also the reduced high-field GKO period that we find in some of our samples. The general lack of support that the variational calculation provides for the heuristic treatment still leaves unanswered at this time the question of why $m^{\dagger}$ and m^{*} differ.

3.3. High-frequency oscillations

The HFO, as illustrated in figure 1, can appear superimposed on the high-field GKO. They vary in intensity from not being visible at all to completely dominating the CPR and high-field GKO, such as happened in sample K-1, for example. When present they generally begin just above CPR, $\omega_c/\omega \simeq 1.05$, reach a maximum amplitude near $\omega_c/\omega = 1.1$ and then fade away by $\omega_c/\omega = 1.3$–1.4. Over most of the field range in which they appear they are linearly spaced in field, although the first few oscillations lie somewhat closer together. In table 1 we give the period ΔH_{HFO} of these oscillations in magnetic field in the linear region for those samples in which they appear. As can be seen from the table, the HFO are visible in only one Na sample, but in a number of the K samples. There is a definite correlation between the presence of the HFO and the sample-preparation techniques, with their appearance being much more likely when the fabrication takes place in argon rather than in vacuum. It thus appears that the rougher, more irregular surfaces favour the appearance of this additional feature.

In figure 4 we plot the period ΔH_{HFO} as a function of the sample thickness L. This is done for all the K and the one Na sample displaying HFO at 80 GHz. Also displayed are the periods of two K samples that were studied with T G Phillips at 116 GHz. As can be seen, there is no obvious dependence on either the material or the applied frequency. Furthermore, there is no clear thickness dependence either. ΔH_{HFO} for all samples but two lies within the range 750 G $\pm$ 20%. Within this band the distribution of points looks to be more or less random. The overall spread of values is certainly much larger than the uncertainties with which they can be determined individually. For all other classes of extended signals seen in the alkali metals, including both single-particle excitations, such as the GKO, and collective-wave modes, such as the SW or CW, there is a very strong dependence of the oscillation period on L. The fact that this is not the case for the HFO plus the larger scatter in the various values of ΔH_{HFO} make them an enigma.

To a considerable degree, the HFO have the same general appearance as the CW

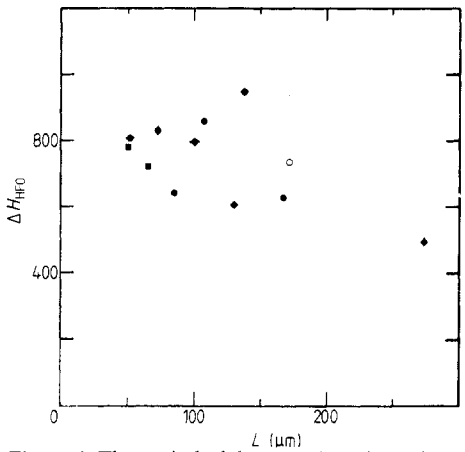

Figure 4. The period of the HFO plotted as a function of the sample thickness L. Note that four different classes of samples are displayed on the plot: ●, K (argon fabrication) at 80 GHz; ◆, K (vacuum fabrication) at 80 GHz; (○), Na (argon fabrication) at 80 GHz; ■, K (argon fabrication) at 116 GHz.

that we studied in the parallel-field geometry (Dunifer *et al* 1987). It is an interesting observation that if one tries to determine an experimental dispersion relation for the HFO by assuming that each complete oscillation corresponds to a change in wavevector $\Delta q = 2\pi/L^*$, then it is possible to choose an effective thickness L^* such that this dispersion relation can be made to coincide with that of either the ordinary- or extraordinary-mode CW (Dunifer *et al* 1979). This includes the small-wavevector portion where significant curvature is present in the dispersion relations. When fitted to the extraordinary-mode dispersion relation, for example, the values of L^* thus calculated vary from approximately 50 to 120 μm and range from 0.5 to 1.5 times the actual sample thickness L. Again, as indicated by the scatter in figure 4, there is no obvious correlation between L and L^*.

Subharmonics of the HFO are seen clearly only for $\omega_c/\omega \simeq \frac{1}{2}$ and only in the samples where the HFO themselves appear on the high-field GKO. Even when present, they are *usually* weak and erratic in appearance, and it is difficult to extract much useful information from them. Samples K-2 and K-4, however, are exceptions, and for these cases it is also possible to fit the subharmonics of the HFO to the dispersion relations of the subharmonics of the CW. This fitting process gives the same value of L^* obtained from the main HFO if they are fitted to the fundamental CW dispersion relation of the *extraordinary* mode. The most convincing case is provided by sample K-2 where two distinct oscillation periods are present in the HFO subharmonic. If it is assumed that these correspond to the ordinary mode and the ω^- branch of the extraordinary mode, then in both cases the same value of L^* is obtained ($\simeq$60 μm) as with the fitting of the main HFO to the fundamental CW dispersion relation. This is approximately 0.6 of the actual thickness of the sample. It is difficult to see how the present geometry of the sample and microwave fields is able to give rise to CW propagation. One possible conjecture is that somehow surface roughness leads to CW propagation parallel to the surface of the sample on the side where the driving fields are present and the CW modes are able to modulate the amplitude of the high-field GKO seen in transmission. If this were the case, it is not clear what would determine the quantity L^*.

3.4. Subharmonics

Superimposed on the low-field GKO in the regions of $\omega_c/\omega \simeq 1/m$, $m = 2, 3, 4, \ldots$, it is possible to see subharmonics of the CPR or HFO. Subharmonics of CPR are seen in almost all samples. In the last column of table 1 we have listed the number of such subharmonics that appear in each sample. As described in the previous section, subharmonics of the HFO are seen clearly only for $m = 2$, and for most samples do not provide much useful information.

From our simple, physical description of the process by which GKO and CPR appear, one would not expect to see subharmonics of the CPR for a material with a spherical Fermi surface. Such subharmonics have been seen, however, in single-crystal copper and silver (Phillips *et al* 1972b), but in this case it is clear that they result from the motion of the electrons around non-circular orbits. In that situation one can always Fourier analyse the motion into a fundamental circular orbit of frequency ω_c plus harmonics consisting of smaller circular orbits of frequency $n\omega_c$, $n = 2, 3, 4, \ldots$. It is generally believed from DHVA studies that the Fermi surface of Na and K differ from sphericity by less than one part in 10^3, and it is not clear whether these small distortions are sufficient to produce subharmonics of the strength detected in our investigation. Other possibilities include the CDW model proposed by Overhauser (1978) that would give rise to larger distortions from sphericity.

4. Conclusions

We have presented the results from an experimental study of microwave transmission through thin plates of Na and K metal carried out at 80 GHz and 1.3 K in the perpendicular-field geometry. The non-spin-related signals consist of Gantmakher–Kaner Oscillations (GKO), cyclotron phase resonance (CPR), high-frequency oscillations (HFO), and subharmonics of CPR and HFO. The physical cause of the GKO and CPR is well understood, but certain details, such as the polarisation, the actual lineshape, the dependence on sample thickness etc, do not appear to be adequately described by current theory. The HFO and the subharmonic signals are not understood at all. The HFO in particular show considerable variation from sample to sample, depend on the method of sample fabrication and may be a spurious effect of some type. The subharmonics of CPR also present an enigma but remain somewhat persistent in the data.

Acknowledgments

Financial support for this research was provided by NSF Grants DMR 7913786 and DMR 8414488, NATO Grant 058.82 and the Departments of Physics at the University of Exeter and Wayne State University. JRS and DAHM also thank the SERC for funding lengthy visits to the USA during which this research was undertaken.

References

Abd El-Rahman A A, Elliott M and Datars W R 1985 *J. Phys. F: Met. Phys.* **15** 859
Baraff G A 1974 *Phys. Rev.* B **9** 4008

Baraff G A, Grimes C C and Platzman P M 1969 *Phys. Rev. Lett.* **22** 590
Cheng Y C, Clarke J S and Mermin N D 1968 *Phys. Rev. Lett.* **20** 1486
Dunifer G L and Pattison M R 1976 *Phys. Rev.* B **14** 945
Dunifer G L, Pinkel D and Schultz S 1974 *Phys. Rev.* B **10** 3159
Dunifer G L, Sambles J R, Mace D A H and Wijeratne A T 1987 *J. Phys. F: Met. Phys.* **17** 1581
Dunifer G L, Schmidt P M and Walsh W M Jr 1979 *Phys. Rev.* B **19** 4918
Elliott M and Datars W R 1982 *J. Phys. F: Met. Phys.* **12** 465
Gantmakher V F and Kaner E A 1965 *Sov. Phys.–JETP* **21** 1053
Lacueva G and Overhauser A W 1986 *Phys. Rev.* B **33** 3765
Mace D A H, Dunifer G L and Sambles J R 1984 *J. Phys. F: Met. Phys.* **14** 2105
Overhauser A W 1978 *Adv. Phys.* **27** 343
Phillips T G, Baraff G A and Dunifer G L 1972a *Phys. Rev. Lett.* **30** 274
Phillips T G, Baraff G A and Schmidt P H 1972b *Phys. Rev.* B **5** 1283
Pines D and Nozieres P 1966 *The Theory of Quantum Liquids* (New York: Benjamin)
Pinkel D, Dunifer G L and Schultz S 1978 *Phys. Rev.* B **18** 6658
Rice T M 1968 *Phys. Rev.* **175** 858